Available online at www.sciencedirect.com
SCIENCE DIRECT®
ELSEVIER
European Journal of Mechanics B/Fluids 22 (2003) 167–178

Linear dynamics of axisymmetric liquid bridges

J.M. Montanero

Departamento de Electrónica e Ingeniería Electromecánica, Universidad de Extremadura, 06071 Badajoz, Spain

Received 10 June 2002; received in revised form 14 February 2003; accepted 27 February 2003

Abstract

The dynamical response of an axisymmetric liquid bridge to small-magnitude perturbations is studied in the framework of the Cosserat model. A numerical procedure to deal with this problem is proposed. The method is found to provide very accurate results from a comparison with the analytical predictions for the cylindrical configuration. The frequencies and damping rates characterizing the oscillation modes are obtained numerically for arbitrary axisymmetric liquid bridge shapes, considering the combined effects of residual gravity, the liquid bridge rotation, the inequality of the disks, and the liquid bridge volume. The results are compared with the predictions obtained from the three-dimensional model for inviscid liquid bridges.

Keywords: Liquid bridge; Linear dynamics; Cosserat model

1. Introduction

Liquid bridges are bodies of fluid anchored between two solid supports and held by capillary forces. The stability and dynamics of liquid bridges has been studied frequently over the past decades both theoretically and experimentally. The theoretical analysis of liquid bridge dynamics involves great difficulties, mainly due to the complex dependence of the surface tension forces on the interface deformation. The integration of the nonlinear equations describing the three-dimensional (hereafter 3-D) problem requires intensive computation [1]. Even in the linear regime, only partial results can be obtained analytically [2–6]. Because of these difficulties, one-dimensional (hereafter 1-D) models have been proposed to study the dynamics of axisymmetric liquid bridges. These models were initially derived for liquid jets and retain integrally the capillary pressure terms. The Cosserat model, derived by Green [7], is a particular case of the so-called mean-velocity models, and accounts partially for radial momentum effects. The relative errors of the Cosserat model associated with the inertial and viscous terms are of the order of λ^{-4} and λ^{-2}, respectively, where λ is defined as the ratio of the typical axial length of the system to the characteristic radial length [8,9]. The Cosserat model has been found to provide accurate predictions in comparisons with 3-D results for slender inviscid liquid bridges [10,11]. However, the relative errors could become noticeable for moderate and large values of the Ohnesorge number.

The expense and difficulty involved in performing space and in-flight experiments have forced researchers to develop experimental support on Earth. In the neutral buoyancy technique (the so-called Plateau-tank simulation), the liquid bridge (made of, for instance, dimethyl-silicone oil) is surrounded by an outer liquid with similar density to partially compensate for the effect of the hydrostatic pressure along the interface [12,13]. In this way, one can obtain stable cylindrical columns of the desired length (taking into account the Rayleigh stability limit). Nevertheless, the theoretical description of such a configuration must account for the influence of the outer bath [2] and of moderate values of the Ohnesorge number. In order to simplify the theoretical model, microzones made of water surrounded by air can be used in experiments. In this case, the influence of the outer bath is negligible and the liquid bridge is near-inviscid. However, if the microzone size is not sufficiently small, gravity produces an amphora-type deformation of the equilibrium shape whose influence on the liquid bridge dynamics is not easy

E-mail address: jmm@unex.es (J.M. Montanero).

0997-7546/03/$ – see front matter
doi:10.1016/S0997-7546(03)00022-0

to determine. Given these experimental conditions, the solution of the Cosserat model for slender liquid bridges is expected to provide good theoretical predictions. The impulsive motion of non-cylindrical liquid bridges has been studied by solving numerically the Cosserat model in the linear regime [14]. The oscillation frequencies and damping rates were found by means of a finite difference scheme as a function of the parameters characterizing the liquid bridge configuration. In the present paper, an accurate numerical procedure is proposed to obtain the oscillation modes of rotating liquid bridges, including their initial amplitudes for an arbitrary time-dependence of the excitation. Also, the results are compared with those obtained from the 3-D model for the inviscid case. The influence of the equilibrium shape on the frequency and damping rate of the first oscillation mode is discussed in detail.

2. Formulation of the problem and mathematical model

The fluid configuration considered is sketched in Fig. 1. It consists of an isothermal mass of liquid of volume $\mathcal{V}$, held between two parallel coaxial disks placed a distance L apart. The radii of the disks are $r_0(1-H)$ and $r_0(1+H)$, r_0 being the mean radius, which is used as the characteristic length. Due to the sharpness of the disk edges, one assumes that the liquid anchors perfectly to those edges, preventing motion of the contact line. Hence, spreading of the liquid over the lateral surfaces of the supporting rods does not occur. The liquid bridge is subjected to the action of a constant axial force (the residual gravity) of magnitude g_0 per unit mass. The liquid bridge density is ρ, the kinematic viscosity is ν, and the surface tension associated with the interface is σ. The liquid bridge is surrounded by another fluid medium of negligible density, so that the external pressure p_{ext} can be considered as constant. The liquid and the disks are solidly rotating at a constant angular speed Ω around the axis of the disks (z axis). For this axisymmetric configuration the equilibrium contour of the liquid bridge is characterized by the function $R_0(z)$, which measures the distance between a surface element and the z axis. Let us now consider the motion produced by the action of an axial force starting at $t=0$, whose magnitude $g(t)$ per unit mass is an arbitrary function of time. The goal is to obtain the function $R(z,t)$, which measures the distance between a surface element and the z axis at the instant t, as well as the velocity field.

The dimensionless space and time coordinates are defined using r_0 and $t_0 \equiv (\rho r_0^3/\sigma)^{1/2}$ as the characteristic length and time, respectively. The dimensionless parameters characterizing the fluid configuration are the slenderness $\Lambda \equiv L/2r_0$, the reduced volume $V \equiv \mathcal{V}/(\pi r_0^2 L)$ (defined as the ratio of the physical volume $\mathcal{V}$ to the volume of a cylinder of the same length L and radius equal to r_0), the residual value of the Bond number $B_0 \equiv \rho g_0 r_0^2/\sigma$, the difference H between the radii of the disks, the Weber number $W \equiv \rho\Omega^2 r_0^3/\sigma$ and the capillary number (defined as the square root of the Ohnesorge number) $C \equiv \nu(\rho/\sigma r_0)^{1/2}$. In addition, the time-dependent Bond number $B(t) \equiv \rho g(t) r_0^2/\sigma$ is a measure of the magnitude of the excitation. The unperturbed shape and the time-dependent contour are characterized by the dimensionless functions $S_0 \equiv R_0^2/r_0^2$ and $S \equiv R^2/r_0^2$, respectively. Finally, let us introduce the dimensionless axial velocity component w and the quantity $Q \equiv Sw$, which is proportional to the axial momentum of a slice of the liquid bridge.

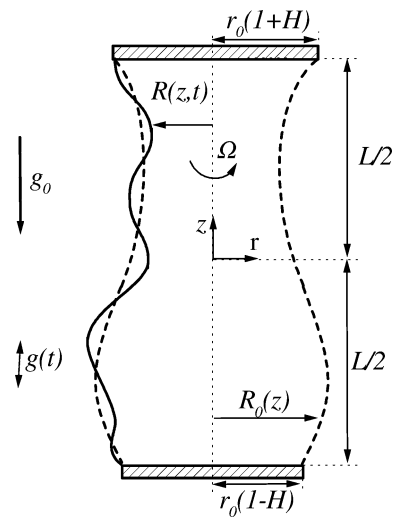

Fig. 1. Geometry and coordinate system for the liquid bridge.

In order to avoid the difficulty of a 3-D description, 1-D models have been considered frequently to obtain theoretical predictions for the liquid bridge problem [8]. In general, these models provide good results as long as the liquid column is slender. As mentioned in the Introduction, the Cosserat model is a particular case of the so-called mean-velocity models. Perales and Meseguer [10] presented a formal procedure for generating the Cosserat model from the Navier–Stokes equations. In this procedure selective terms were retained in a perturbation expansion. Also, Schulkes [15] demonstrated that the Cosserat model can be derived by means of a consistent approximation of the Euler equations for the inviscid case. In both cases the rotation of the liquid bridge was not considered. The extension of these procedures to take into account the role played by the Weber number is trivial. The Cosserat model as applied to the rotating liquid bridge problem reduces to the continuity equation

$$S_t + Q_z = 0, \tag{1a}$$

the momentum equation

$$\mathcal{D}S - \frac{1}{8}\left\{S^2\left[\mathcal{D}_z - \frac{3}{2}\left(\frac{Q}{S}\right)_z^2\right]\right\}_z = -SP_{cz} - \frac{1}{8}C\left[S^2\left(\frac{Q}{S}\right)_{zz}\right]_{zz} + 3C\left[S\left(\frac{Q}{S}\right)_z\right]_z, \tag{1b}$$

the boundary conditions at the solid surfaces

$$Q(\pm\Lambda, t) = 0, \tag{1c}$$

and the condition of anchorage at the disks

$$S(\pm\Lambda, t) = (1 \pm H)^2. \tag{1d}$$

In the above equations and hereafter, a subscript denotes the partial derivative with respect to the corresponding variable. In Eq. (1b), $\mathcal{D} \equiv [Q_t + (Q^2/S)_z]/S$, and P_c includes both hydrostatic and capillary pressures:

$$P_c = 4\left(2S + S_z^2 - SS_{zz}\right)\left(4S + S_z^2\right)^{-3/2} + B_0 z - \frac{1}{2}WS + B(t)z. \tag{1e}$$

Finally, the initial conditions are

$$Q(z, 0) = 0, \qquad S(z, 0) = S_0(z). \tag{1f}$$

The rotation of the liquid bridge and the disks as a solid body produces a centrifugal force that (as occurs with gravity) can be eliminated formally from the momentum equation in the 3-D model. The term associated with this force only appears in the formulation through the quantity P_c when one considers the normal stress equilibrium of the interface [10,15]. In addition, the axial and radial components of the Coriolis force vanish for axisymmetric perturbations. Therefore, one can obtain the 1-D Cosserat for rotating liquid bridges model from the Navier–Stokes (Euler) equations following the same procedures as those exposed in [10,15].

3. Linear analysis

Consider now the influence of the small-magnitude excitation force

$$B(t) = \varepsilon b(t), \tag{2a}$$

where $\varepsilon \ll 1$ is a perturbation parameter and $b(t)$ is an arbitrary function of time which vanishes for $t \leqslant 0$. The functions $S(z, t)$ and $Q(z, t)$ describing the dynamical response of the liquid bridge can be expanded as

$$S(z, t) = S_0(z) + \varepsilon s(z, t) + \mathcal{O}\left(\varepsilon^2\right), \tag{2b}$$

$$Q(z, t) = \varepsilon q(z, t) + \mathcal{O}\left(\varepsilon^2\right). \tag{2c}$$

The function $S_0(z)$ is obtained from the zeroth-order problem:

$$4\left(2S_0 + S_{0z}^2 - S_0 S_{0zz}\right)\left(4S_0 + S_{0z}^2\right)^{-3/2} + B_0 z - \frac{1}{2}WS_0 = \widehat{P}_0, \tag{3a}$$

$$S_0(\pm\Lambda) = (1 \pm H)^2. \tag{3b}$$

The constant $\widehat{P}_0$ appearing in Eq. (3a) is the capillary pressure, and can be calculated by considering the condition

$$\int_{-\Lambda}^{\Lambda} S_0 \,\mathrm{d}z = 2\Lambda V. \tag{3c}$$

The first-order problem yields

$$s_t + q_z = 0, \tag{4a}$$

$$q_t - \frac{1}{8}(S_0 q_{tzz} - S_{0zz} q_t) = D_0 s + D_1 s_z + D_2 s_{zz} + D_3 s_{zzz} + S_0 b - \frac{1}{8} C\left[S_0^2\left(\frac{q}{S_0}\right)_{zz}\right]_{zz} + 3C\left[S_0\left(\frac{q}{S_0}\right)_z\right]_z, \tag{4b}$$

$$q(\pm\Lambda, t) = 0, \qquad s(\pm\Lambda, t) = 0, \tag{4c}$$

$$q(z, 0) = 0, \qquad (z, 0) = 0. \tag{4d}$$

The functions $D_i(z)$ appearing in (4b) are calculated in terms of S_0 and its derivatives from the perturbation expansion of $-SP_{cz}$. The results are

$$D_0 = \frac{8}{(4S_0 + S_{0z}^2)^{7/2}}\big[S_{0z}^5(2 + S_{0zz}) + 4S_0^3 S_{0zzz} + S_0 S_{0z}^3(-8 - 10S_{0zz} - 3S_{0zz}^2 + S_{0z}S_{0zzz}) + S_0^2 S_{0z}(-4 + 4S_{0zz} + 3S_{0zz}^2 + 5S_{0z}S_{0zzz})\big] + \frac{1}{2}S_{0z}W, \tag{5a}$$

$$D_1 = \frac{4S_0}{(4S_0 + S_{0z}^2)^{7/2}}\big[-4S_{0z}^4(2 + S_{0zz}) + S_0 S_{0z}^2(32 + 40S_{0zz} + 12S_{0zz}^2 - 3S_{0z}S_{0zzz}) - 4S_0^2(-4 + 4S_{0zz} + 3S_{0zz}^2 + 3S_{0z}S_{0zzz})\big] + \frac{1}{2}S_0 W, \tag{5b}$$

$$D_2 = -\frac{8S_0 S_{0z}[-S_{0z}^2 + S_0(2 + 3S_{0zz})]}{(4S_0 + S_{0z}^2)^{5/2}}, \tag{5c}$$

$$D_3 = \frac{4S_0^2}{(4S_0 + S_{0z}^2)^{3/2}}. \tag{5d}$$

The function s can be eliminated from the formulation by considering the continuity equation (4a). The result is

$$q_{tt} - \frac{1}{8}(S_0 q_{ttzz} - S_{0zz} q_{tt}) = -D_0 q_z - D_1 q_{zz} - D_2 q_{zzz} - D_3 q_{zzzz} + S_0 b_t + E_0 q_t + E_1 q_{tz} + E_2 q_{tzz} + E_3 q_{tzzz} + E_4 q_{tzzzz}, \tag{6a}$$

$$q(\pm\Lambda, t) = 0, \tag{6b}$$

$$q_z(\pm\Lambda, t) = 0, \tag{6c}$$

$$q(z, 0) = 0, \tag{6d}$$

$$q_t(z, 0) = 0. \tag{6e}$$

The functions $E_i(z)$ are obtained from the linearization of the viscosity terms, i.e.,

$$E_0 = \frac{C}{8S_0^3}\big[S_0^3 S_{0zzzz} - 4S_{0z}^4 + 2S_0 S_{0z}^2(12 + 5S_{0zz}) - 4S_0^2(6S_{0zz} + S_{0zz}^2 + S_{0z}S_{0zzz})\big], \tag{7a}$$

$$E_1 = \frac{C}{2S_0^2}\big[S_{0z}^3 - 2S_0 S_{0z}(3 + S_{0zz}) + S_0^2 S_{0zzz}\big], \tag{7b}$$

$$E_2 = \frac{C}{2}\left[6 + S_{0zz} - \frac{S_{0z}^2}{2S_0}\right], \tag{7c}$$

$$E_3 = 0, \tag{7d}$$

$$E_4 = -\frac{C}{8}S_0. \tag{7e}$$

The initial condition (6e) is deduced by considering Eq. (4b) at $t = 0$ and the conditions (4d).

Let $\mathcal{Q}(z, h)$ be the Laplace transform of $q(z, t)$. Taking into account the initial conditions (6d) and (6e), Eqs. (6a)–(6c) yield

$$F_0(z, h)\mathcal{Q} + F_1(z, h)\mathcal{Q}_z + F_2(z, h)\mathcal{Q}_{zz} + F_3(z, h)\mathcal{Q}_{zzz} + F_4(z, h)\mathcal{Q}_{zzzz} + S_0(z)\mathcal{B}(h) = 0, \tag{8a}$$

$$\mathcal{Q}(\pm\Lambda, h) = 0, \tag{8b}$$

$$\mathcal{Q}_z(\pm\Lambda, h) = 0, \tag{8c}$$

where $F_0 = hE_0 - h^2(1/8\ S_{0zz} + 1)$, $F_1 = hE_1 - D_0$, $F_2 = h^2/8S_0 + hE_2 - D_1$, $F_3 = hE_3 - D_2$, $F_4 = hE_4 - D_3$, and $\mathcal{B}(h)$ is the Laplace transform of $b_t(t)$. The function $\mathcal{Q}(z,h)$ can be calculated numerically from (8). Once the value of $\mathcal{Q}$ is known, the Laplace transform $\mathcal{S}(z,h)$ of $s(z,t)$ is obtained from the continuity equation, i.e.,

$$\mathcal{S}(z,h) = -\frac{1}{h}\mathcal{Q}_z(z,h). \tag{9}$$

The inverse transform of $\mathcal{Q}(z,h)$ can be calculated by finding the poles and evaluating the corresponding residues [16]. Assuming that $\mathcal{Q}(z,h)$ has no poles at $h=0$, the velocity field $q(z,t)$ can be written as

$$q(z,t) = \sum_{p=1}^{\infty} A_q^{(p)}(z)\exp(h_p t), \tag{10}$$

where $A_q^{(p)}(z) = \lim_{h\to h_p}(h-h_p)\mathcal{Q}(z,h)$, and h_p are the (simple) poles of $\mathcal{Q}(z,h)$. Given the relation (9) between $\mathcal{S}(z,h)$ and $\mathcal{Q}(z,h)$, $\mathcal{S}(z,h)$ could have a simple pole at $h=0$. Therefore, the inverse transform of $\mathcal{S}$ must be written, in general, as

$$s(z,t) = A_s^{(0)}(z) + \sum_{p=1}^{\infty} A_s^{(p)}(z)\exp(h_p t), \tag{11}$$

where $A_s^{(0)}(z) = \lim_{h\to 0} h\mathcal{S}(z,h)$, and $A_s^{(p)}(z) = \lim_{h\to h_p}(h-h_p)\mathcal{S}(z,h)$.

One can find an infinite set of poles h_p which do not depend on the excitation function $\mathcal{B}(h)$. These poles characterize the oscillation modes of the system [14,17,18]. The functions $A_q^{(p)}(z)$ and $A_s^{(p)}(z)$ are the corresponding initial amplitudes of the velocity field and of the contour deformation, respectively, for a given function $\mathcal{B}(h)$. Because $q(z,t)$ and $s(z,t)$ must be real functions, these poles and amplitudes appear either as pairs of conjugate values or as real numbers. More precisely, if $p < p_c$ then the poles and the amplitudes appear as pairs of conjugate values, and if $p \geqslant p_c$ then they are real numbers. The critical value p_c depends on the parameters characterizing the liquid bridge. In particular, the value of p_c decreases as the capillary number C increases. In other words, for a given value of p, there exists a critical value of the capillary number, $C_c^{(p)}$, such that if $C < C_c^{(p)}$ then h_p, $A_q^{(p)}$ and $A_s^{(p)}$ are the conjugate values of their corresponding pairs, and if $C \geqslant C_c^{(p)}$ then they are real numbers. The values of $C_c^{(p)}$ depend on the parameters characterizing the fluid configuration (Λ, V, B_0, H, W). For the particular case $C=0$, $h_p = \pm i\omega_p$ for all p, and the set of values ω_p must be identified as the resonance frequencies of the system.

It must be noticed that the poles, if they exist, of the excitation function $\mathcal{B}(h)$ are additional poles of $\mathcal{Q}(z,h)$, and hence they must also be considered. For instance, when the excitation force is an oscillatory microgravity field of frequency ω, $h_p = \pm i\omega$ are poles of $\mathcal{B}(h)$, and thus of $\mathcal{Q}(z,h)$. This example will be discussed in detail in Section 4 for the cylindrical configuration.

4. Analytical results for cylindrical liquid bridges

In general, the coefficients $F_i(z,h)$ appearing in Eq. (8a) are to be calculated numerically from the knowledge of $S_0(z)$ and its derivatives. However, for the particular case $V-1 = B_0 = H = 0$, $S_0 = 1$, and (8a) becomes

$$\left(\frac{1}{2} + \frac{1}{8}hC\right)\mathcal{Q}_{zzzz} + \left(\frac{1}{2} + \frac{1}{2}W - \frac{1}{8}h^2 - 3hC\right)\mathcal{Q}_{zz} + h^2\mathcal{Q} + \mathcal{B} = 0. \tag{12}$$

The solution of the above differential equation with the boundary conditions (8b) and (8c) is

$$\mathcal{Q}(z,h) = \frac{\mathcal{B}(h)}{h^2}\frac{D(z,h) - D(\Lambda,h)}{D(\Lambda,h)}, \tag{13a}$$

where

$$D(z,h) = \theta_2\sinh(\theta_2\Lambda)\cosh(\theta_1 z) - \theta_1\sinh(\theta_1\Lambda)\cosh(\theta_2 z), \tag{13b}$$

$$\theta_{1,2}^2 = \frac{-1 + h^2/4 - W + 6hC}{2 + hC/2} \pm \frac{[-2h^2(4+hC) + (4 - 24hC - h^2 + 4W)^2/16]^{1/2}}{2 + hC/2}. \tag{13c}$$

The signs $+$ and $-$ correspond to θ_1 and θ_2, respectively. The Laplace transform of the interface deformation $s(z,t)$ is

$$\mathcal{S}(z,h) = -\frac{\mathcal{B}(h)}{h^3}\frac{D_z(z,h)}{D(\Lambda,h)}. \tag{13d}$$

The solution (13) was obtained in [17] for the particular case $W = 0$.

Assuming that $\mathcal{Q}(z, h)$ has no poles at $h = 0$, the inverse transform of (13a) can be written as

$$q(z,t) = \sum_p \frac{D(z,h_p^*) - D(\Lambda,h_p^*)}{h_p^{*2}(\mathcal{B}^{-1})_h(h_p^*)\ D(\Lambda,h_p^*)} \exp(h_p^* t) + \sum_{p=1}^{\infty} \frac{\mathcal{B}(h_p) D(z,h_p)}{h_p^2 D_h(\Lambda,h_p)} \exp(h_p t), \tag{14a}$$

where h_p^* are, if they exist, the poles of $\mathcal{B}$. Here, h_p are the roots of $D(\Lambda, h) = 0$, and characterize the oscillation modes of the cylindrical liquid bridge. The inverse transform of $\mathcal{S}(z, h)$ is

$$s(z,t) = A_s^{(0)}(z) - \sum_p \frac{D_z(z,h_p^*)}{h_p^{*3}(\mathcal{B}^{-1})_h(h_p^*) D(\Lambda,h_p^*)} \exp(h_p^* t) - \sum_{p=1}^{\infty} \frac{\mathcal{B}(h_p) D_z(z,h_p)}{h_p^3 D_h(\Lambda,h_p)} \exp(h_p t), \tag{14b}$$

where $A_s^{(0)}(z) = \lim_{h\to 0} h\mathcal{S}(z, h)$.

Different liquid bridge motions can be analysed using the above formulae. In the impulsive motion, one studies the dynamical response of the liquid column to an excitation consisting of a small change in the value of the microgravity level at $t = 0$ [17]. Therefore, $b(t) = \mathcal{H}(t)$, $\mathcal{H}(t)$ being the Heaviside function [$\mathcal{H}(t) = 0$ for $t \leqslant 0$ and $\mathcal{H}(t) = 1$ for $t > 0$], $b_t(t) = \delta(t)$, where $\delta(t)$ is the Dirac delta function, $\mathcal{B}(h) = 1$,

$$q(z,t) = \sum_{p=1}^{\infty} \frac{D(z,h_p)}{h_p^2 D_h(\Lambda,h_p)} \exp(h_p t), \tag{15a}$$

$$s(z,t) = A_s^{(0)}(z) - \sum_{p=1}^{\infty} \frac{D_z(z,h_p)}{h_p^3 D_h(\Lambda,h_p)} \exp(h_p t). \tag{15b}$$

Here, the function $A_s^{(0)}(z) = 2(z - \Lambda \sin z/\sin\Lambda)$ is the linear perturbation of the equilibrium contour due to the presence of axial gravity.

The most common disturbances on board space platforms are those produced by single events, such as pulse-like accelerations due to a docking activity, crew movement, operation of equipment on the space station, etc. [19]. Let us now consider the perturbation produced by a g-pulse that occurs during the interval $0 < t \leqslant t_0$. In this case, $b(t) = \mathcal{H}(t) - \mathcal{H}(t - t_0)$, $b_t(t) = \delta(t) - \delta(t - t_0)$, $\mathcal{B}(h) = 1 - \exp(-ht_0)$,

$$q(z,t) = \sum_{p=1}^{\infty} \big[1 - \exp(h_p t_0)\big] \frac{D(z,h_p)}{h_p^2 D_h(\Lambda,h_p)} \exp(h_p t), \tag{16a}$$

$$s(z,t) = \sum_{p=1}^{\infty} \big[\exp(h_p t_0) - 1\big] \frac{D_z(z,h_p)}{h_p^3 D_h(\Lambda,h_p)} \exp(h_p t). \tag{16b}$$

Consider now the action of an oscillatory microgravity field (due to, for instance, an in-phase vibration of the supporting disks). In this case, $b(t) = \sin(\omega t)$ (for $t \geqslant 0$), ω being the angular speed, $b_t = \omega\cos(\omega t)$, $\mathcal{B}(h) = h\omega/(h^2 + \omega^2)$, $h_{1,2}^* = \pm i\omega$,

$$q(z,t) = \frac{1}{\omega}\left[1 - \frac{D(z,i\omega)}{D(\Lambda,i\omega)}\right]\cos(\omega t) + \sum_{p=1}^{\infty} \frac{\omega}{h_p^2 + \omega^2} \frac{D(z,h_p)}{h_p D_h(\Lambda,h_p)} \exp(h_p t), \tag{17a}$$

$$s(z,t) = \frac{1}{\omega^2} \frac{D_z(z,i\omega)}{D(\Lambda,i\omega)} \sin(\omega t) - \sum_{p=1}^{\infty} \frac{\omega}{h_p^2 + \omega^2} \frac{D_z(z,h_p)}{h_p^2 D_h(\Lambda,h_p)} \exp(h_p t). \tag{17b}$$

It can be verified that the first contributions to $q(z, t)$ and $s(z, t)$ given by (17a) and (17b), respectively, are the sum of the terms associated with the poles $h_{1,2}^* = \pm i\omega$. If $C > 0$, the terms included in the summations of (17a) and (17b) are damped, and hence the first contributions mentioned above correspond to the long-time solution [10,11]. For $C = 0$, $h_p = \pm i\omega_p$ for all p, and hence if $\omega = \omega_p$ then $D(\Lambda, i\omega) = 0$, and the functions $q(z, t)$ and $s(z, t)$ tend to infinity. Those values of the angular speed correspond to the resonance frequencies of the system.

5. Numerical scheme

The set of Eqs. (8) constitutes a typical two-point boundary-value problem that can be solved using different techniques. For instance, a finite difference scheme has been developed to deal with this numerical problem for $W = 0$ [14]. In this paper, the problem (8) is solved by transforming it to an initial-value problem, avoiding the errors associated with discretization. First, the calculation of the liquid bridge equilibrium shape is performed by solving the problem (3) [13]. Once the value of the function $S_0(z)$ has been obtained, the differential equation (8a) is numerically integrated by means of a fifth-order Runge–Kutta method. The secant method is used to find the values of $\mathcal{Q}_{zz}(-\Lambda, h)$ and $\mathcal{Q}_{zzz}(-\Lambda, h)$ that lead to $\mathcal{Q}(\Lambda, h) = \mathcal{Q}_z(\Lambda, h) = 0$. The algorithm considers the solution (13a) for the cylinder as initial guess. The value of $\mathcal{S}(\Lambda, h)$ is easily obtained from the continuity equation (9).

Due to the linearity of (8a), the Jacobian J of the transformation $\{\mathcal{Q}_{zz}(-\Lambda, h),\ \mathcal{Q}_{zzz}(-\Lambda, h)\} \to \{\mathcal{Q}(\Lambda, h), \mathcal{Q}_z(\Lambda, h)\}$ only depends on the value of h (and on the values of the parameters characterizing the liquid bridge). The roots of $J(h) = 0$ must be identified as the poles of $\mathcal{Q}(z, h)$ characterizing the oscillation modes of the system. These roots can be easily found by means of a variant of the secant-method, using as initial guess a solution previously calculated for a similar configuration. Once the values of the poles have been obtained, the initial amplitudes $A_q^{(p)}(z)$ and $A_s^{(p)}(z)$ are calculated by estimating the corresponding limit. First, a short sequence of values of the functions $(h - h_p)\mathcal{Q}(z, h)$ and $(h - h_p)\mathcal{S}(z, h)$ are evaluated as the argument h approaches the pole h_p. Then, a routine that uses either Wynn's algorithm or a generalized Euler transformation is used to find an approximation to the limit [20]. The function $A_s^{(0)}(z)$ can be obtained by following the same procedure. The Laplace transforms $\mathcal{Q}(z, h)$ and $\mathcal{S}(z, h)$ can also be numerically inverted by means of the Fourier-series method [16,21]. The resulting infinite series are calculated approximately using the Euler algorithm [21].

The numerical procedure described above was tested by comparing the results obtained for cylindrical liquid bridges with those calculated from the analytical solution. Tables 1 and 2 show the values of the first four poles and the corresponding initial amplitudes at $z = \Lambda/4$ for $\mathcal{B}(h) = 1$ (impulsive motion) obtained from the two methods and for different values of the capillary number C and Weber number W. The agreement for the poles h_p is excellent, while the discrepancies observed for the initial amplitudes are larger. These discrepancies are due to approximations in the numerical estimation of the limit. Fig. 2 shows the values of $q(z = -\Lambda/2, t = 10)$ for two inviscid cylindrical liquid bridges subjected to an impulsive motion. The dashed lines represent the values obtained from the numerical procedure using the Fourier-series method together with the Euler algorithm for inverting $\mathcal{Q}(z, h)$. The symbols correspond to the analytical solution calculated by considering n oscillation modes. Because $C = 0$, the oscillation modes are not damped, and their relative influence on the value of q does not depend on the time t. The differences observed between the numerical predictions and the analytical results for $n = 14$ are smaller than 0.3%. These discrepancies are probably due to truncation errors in the Euler sum. In addition, the computational efficiency of the Fourier-series method decreases as t decreases.

One can conclude that the numerical method proposed provides accurate results from comparison with the analytical solution for cylindrical liquid bridges. Given that the mathematical structure of the problem is the same for cylindrical and

Table 1
Poles h_p and initial amplitudes $A_s^{(p)}(z = \Lambda/4)$ for $\mathcal{B}(h) = 1$, $\Lambda = 2$, $V - 1 = B_0 = H = 0$, and for $W = 0$ as a function of the capillary number C. The upper (lower) values are the results obtained from the analytical solution (numerical method)

C	$h_{1,2}$	$A_s^{(1,2)}(z = \Lambda/4)$
0	$\pm 0.732328\mathrm{i}$	0.5833
	$\pm 0.732329\mathrm{i}$	$0.5832 \mp 10^{-4}\mathrm{i}$
0.1	$-0.119044 \pm 0.723155\mathrm{i}$	$0.5826 \mp 0.1078\mathrm{i}$
	$-0.119044 \pm 0.723151\mathrm{i}$	$0.5824 \mp 0.1079\mathrm{i}$
0.2	$-0.239049 \pm 0.694708\mathrm{i}$	$0.580 \mp 0.226\mathrm{i}$
	$-0.239049 \pm 0.694709\mathrm{i}$	$0.581 \mp 0.224\mathrm{i}$
C	$h_{3,4}$	$A_s^{(3,4)}(z = \Lambda/4)$
0	$\pm 3.78920\mathrm{i}$	-0.03284
	$\pm 3.78920\mathrm{i}$	$-0.03284 \pm 2 \times 10^{-5}\mathrm{i}$
0.1	$-0.723173 \pm 3.71821\mathrm{i}$	$-0.03202 \pm 0.0089\mathrm{i}$
	$-0.723176 \pm 3.71823\mathrm{i}$	$-0.03203 \pm 0.0088\mathrm{i}$
0.2	$-1.44723 \pm 3.49615\mathrm{i}$	$-0.0293 \pm 0.0184\mathrm{i}$
	$-1.44725 \pm 3.49620\mathrm{i}$	$-0.0294 \pm 0.0182\mathrm{i}$

Table 2
The same as Table 1 but for $W = 0.2$

C	$h_{1,2}$	$A_s^{(1,2)}(z = \Lambda/4)$
0	$\pm 0.681429\mathrm{i}$	0.67958
	$\pm 0.681427\mathrm{i}$	$0.67957 \mp 5 \times 10^{-4}\mathrm{i}$
0.1	$-0.119555 \pm 0.671426\mathrm{i}$	$0.678 \mp 0.134\mathrm{i}$
	$-0.119556 \pm 0.671429\mathrm{i}$	$0.679 \mp 0.130\mathrm{i}$
0.2	$-0.240175 \pm 0.64020\mathrm{i}$	$0.676 \mp 0.284\mathrm{i}$
	$-0.240175 \pm 0.64022\mathrm{i}$	$0.679 \mp 0.280\mathrm{i}$
C	$h_{3,4}$	$A_s^{(3,4)}(z = \Lambda/4)$
0	$\pm 3.74303\mathrm{i}$	-0.033893
	$\pm 3.74304\mathrm{i}$	$-0.033894 \pm 4 \times 10^{-5}\mathrm{i}$
0.1	$-0.722935 \pm 3.67106\mathrm{i}$	$-0.0330 \pm 0.0090\mathrm{i}$
	$-0.722947 \pm 3.67108\mathrm{i}$	$-0.0328 \pm 0.0094\mathrm{i}$
0.2	$-1.44673 \pm 3.44567\mathrm{i}$	$-0.03013 \pm 0.0194\mathrm{i}$
	$-1.44676 \pm 3.44572\mathrm{i}$	$-0.03013 \pm 0.0186\mathrm{i}$

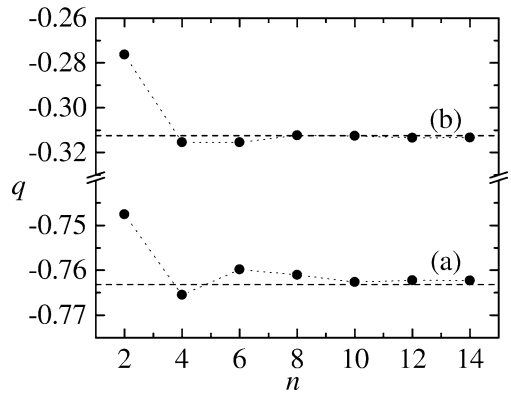

Fig. 2. Values of $q(z = -\Lambda/2, t = 10)$ for $\mathcal{B}(h) = 1$, $V - 1 = B_0 = H = C = 0$, and $\Lambda = 2$, $W = 0$ (a), and $\Lambda = 1.5$ and $W = 0.5$ (b). The dashed lines are the values obtained from the numerical procedure using the Fourier-series method together with the Euler algorithm. The symbols are the analytical solution calculated by considering n oscillation modes.

non-cylindrical shapes, and the functions $F_i(z, h)$ are calculated accurately for arbitrary equilibrium contours, the validity of the numerical scheme can also be expected to hold for those configurations.

6. Results

The predictions obtained from the 1-D Cosserat model are expected to be in good agreement with 3-D results provided that the slenderness of the liquid bridge is not small ($\Lambda \gtrsim 1$) and the capillary number takes small values ($C \lesssim 0.05$). In [11], the dynamical response of inviscid liquid bridges to an oscillatory microgravity field is analysed by means of the 3-D model considering the combined effect of residual gravity, the liquid bridge volume, the inequality of the disks, and the liquid bridge rotation but neglecting the Coriolis force. The adaptation of both the analytical and the numerical procedures used in that reference to calculate now the poles h_p for $C = 0$ is straightforward. For cylindrical liquid bridges, the poles h_p are those verifying the condition

$$\tilde{\Lambda} \tan \tilde{\Lambda} - 2\tilde{h}_p^2 \sum_{\substack{n=1 \\ n \text{ odd}}}^{\infty} \ell_n \big[j_n - \tilde{h}_p^2 I_0\big(k_n \widetilde{W}\big) \big]^{-1} = 0, \tag{18}$$

where $\tilde{\Lambda} \equiv \Lambda \widetilde{W}$, $\widetilde{W} \equiv (1 + W)^{1/2}$, $\tilde{h}_p \equiv h_p \widetilde{W}^{-3/2}$, $\ell_n = I_0(k_n \widetilde{W})/1 - k_n^2$, $k_n = n\pi/2\tilde{\Lambda}$, $j_n = k_n(1 - k_n^2) I_1(k_n \widetilde{W})$, and $I_0(x)$ and $I_1(x)$ are the modified Bessel functions of zeroth and first-order, respectively. The numerical scheme used here to calculate the poles $h_{1,2}$ characterizing the first oscillation mode of non-cylindrical liquid bridges is formally identical to that described in

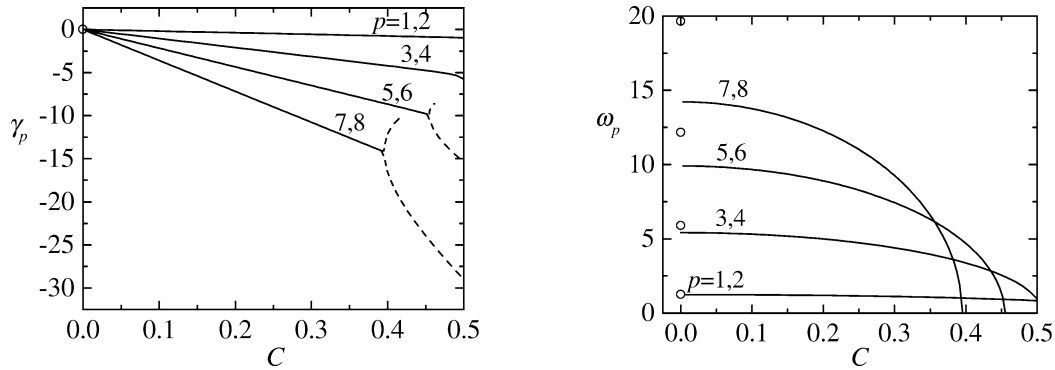

Fig. 3. First poles $h_p = \gamma_p \pm \mathrm{i}\omega_p$ as a function of the capillary number C for $\Lambda = 1.6$, $B_0 = H = W = 0$ obtained from the Cosserat model (lines) and from the 3-D model for $C = 0$ (symbols). Solid lines with the same labels in the two graphs indicate the conjugate values $h_p = \gamma_p \pm \mathrm{i}\omega_p$ of a pair of poles. The dashed lines in the left-hand graph show the values of the real poles.

Ref. [11] for obtaining the first resonance frequency of the system. Basically, the method is an iterative scheme consisting of two steps. First, for an initial value of $\mathcal{S}(z,h)$, the Laplace transform of the velocity potential, $\Phi(r,z,h)$, is calculated by integrating the Laplace equation with the boundary conditions at the disks, at the axis of symmetry (z axis), and at the interface (the kinematic compatibility). The integration is performed using a finite-difference scheme. Second, once $\Phi(r,z,h)$ is obtained, the value of $\mathcal{S}(z,h)$ is updated by integrating the capillary equation and taking into account the condition of anchorage at the disks and volume conservation. The algorithm goes back to the first step but now considering the updated value of $\mathcal{S}(z,h)$. This procedure is iterated until the values of $\mathcal{S}(z,h)$ and $\Phi(r,z,h)$ converge to the required precision. The poles $h_{1,2}$ are those values of h for which the maximum of $\mathcal{S}(z,h)$ reaches a certain value.

Fig. 3 shows the poles h_p corresponding to the first eight modes of a cylindrical liquid bridge as a function of the capillary number C. The lines correspond to the solution of the Cosserat model obtained by finding the roots of $D(\Lambda,h) = 0$, where the function $D(z,h)$ is given by (13b). Solid lines with the same labels in the two graphs indicate the conjugate values $h_p = \gamma_p \pm \mathrm{i}\omega_p$ of a pair of poles. The dashed lines in the left-hand graph show the values of the real poles. The symbols represent the first eight poles calculated by means of the 3-D model for $C = 0$. As can be observed, for each value of the capillary number C the poles appear as pairs of conjugate values if $p < p_c$, and are real numbers otherwise. The critical value p_c decreases as the capillary number C increases. For instance, $p_c = 7$ for $C = 0.42$, and $p_c = 5$ for $C = 0.47$. In addition, for each value of the index p there exists a critical value $C_c^{(p)}$ of the capillary number C such that for $C = C_c^{(p)}$, $\omega_p = 0$. For the liquid bridge considered in Fig. 3, one gets $C_c^{(1,2)} \simeq 0.638$, $C_c^{(3,4)} \simeq 0.550$, $C_c^{(5,6)} \simeq 0.455$ and $C_c^{(7,8)} \simeq 0.395$. For small (moderate) values of the capillary number, the magnitude of γ_p increases sharply as the value of the index p increases and as the capillary number C increases. The agreement between the predictions obtained from the 3-D and the Cosserat models for the first resonance frequency is quite good, but worsens as p increases. As said in the Introduction, the relative error of the Cosserat model increases as λ decreases, where λ is the ratio of a typical axial length to the characteristic radial length. As the index p increases, the number of nodes of the corresponding oscillation mode also increases, and hence the value of λ associated with that mode decreases. This explains why increasing p leads to greater discrepancies between the results obtained from the 3-D and 1-D models.

The most significant oscillation mode is the first for two reasons. First, the magnitude of the initial amplitudes $A_q^{(p)}$ and $A_s^{(p)}$ decreases rapidly as the value of the index p increases (see, for instance, Tables 1 and 2). These quantities indicate the relative relevance of the different oscillation modes for any time if $C = 0$, and for short times if $C \neq 0$. Second, if $C \neq 0$, the oscillation modes are damped much faster as p increases (see, for instance, the values of γ_p in Tables 1 and 2 and in Fig. 3). Therefore, for viscous liquid bridges the relative influence of the first oscillation mode increases with time. In what follows, only the first oscillation mode will be considered, and results for the poles $h_{1,2}$ will be presented for different choices of the parameters characterizing the liquid bridge configuration.

Nicolás and Vega [6] calculated the damping rate and the frequency of the first oscillation mode for non-rotating cylindrical liquid bridges by using the 3-D model. Fig. 4 shows a comparison between the results obtained in that work for $\Lambda = \pi/4$ and those calculated from the condition $D(\Lambda,h) = 0$. In spite of the fact that liquid bridge cannot be considered slender, the 1-D predictions are in good agreement with the 3-D model independently of the viscosity value. For the liquid bridge considered in the figure, the critical value of the capillary number is $C_c^{(1,2)} \simeq 0.568$. Only the dominant damping rate is plotted for $C > C_c^{(1,2)}$. Fig. 5 shows the dependence of $h_1 = \gamma_1 + \mathrm{i}\omega_1$ on the slenderness Λ for $V - 1 = H = 0$, $B_a = 0.05$, and $W = 0.2$. The symbols

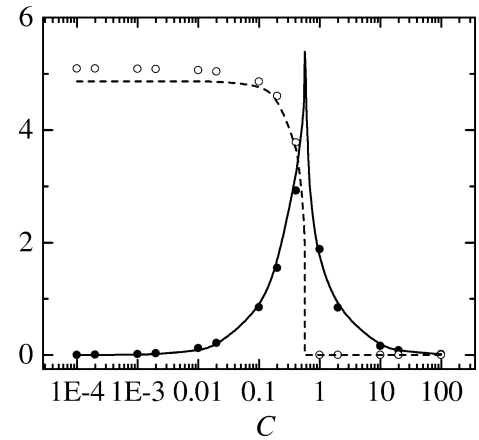

Fig. 4. Dumping rate $-\gamma_1$ (solid line and ●) and frequency ω_1 (dashed line and ○) as a function of the capillary number C for $\Lambda = \pi/4$, $B_0 = H = W = 0$ obtained from the Cosserat model (lines) and from the 3-D model (symbols) [6].

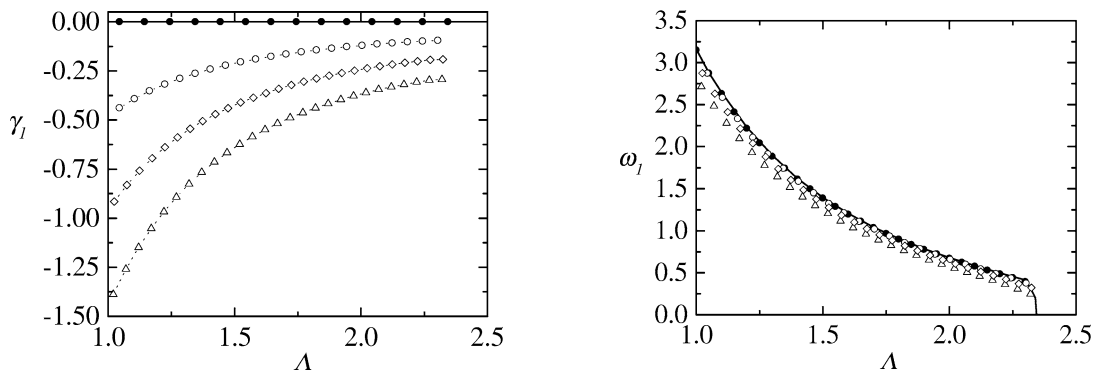

Fig. 5. Pole $h_1 = \gamma_1 + \mathrm{i}\omega_1$ as a function of the slenderness Λ for $V = 1$, $B_0 = 0.05$, $H = 0$ and $W = 0.2$. The symbols are the results obtained from the Cosserat model for $C = 0$ (●), 0.1 (○), 0.2 (◇) and 0.3 (△), while the solid lines represent the results obtained by means of the 3-D model for $C = 0$.

correspond to the results obtained from the Cosserat model for different values of the capillary number C, while the solid lines are the predictions calculated using the 3-D model for $C = 0$. The magnitude of the damping rate γ_1 increases as the slenderness decreases, showing that the damping effect due to viscosity is larger for shorter liquid bridges. There is notable agreement between the results obtained by means of the Cosserat and the 3-D models for $C = 0$. In this case, the Cosserat model accounts correctly for the influence of the radial component of the velocity field on the liquid bridge dynamics. Near the stability limit, the capillary force decreases much more rapidly than viscous stresses as Λ increases, so that the viscosity force dominates the liquid bridge dynamics. This explains why the poles become real near that limit and why the frequency ω_1 decreases sharply as C increases, until it becomes zero for $C = C_c^{(1,2)}$. Fig. 6 shows the dependence of the first pole on the liquid bridge volume. The influence of this quantity is significant, especially in the case of the frequency ω_1. The magnitude of the damping rate γ_1 increases notably as the capillary number C increases. As also shown in Fig. 5 with respect to the slenderness Λ, ω_1 is practically independent of the viscosity over a wide range of volume values. However, near the stability limit of minimum volume the effect of the capillary number becomes more evident. The agreement between the results obtained from the Cosserat and the 3-D models for $C = 0$ is quite good. Finally, in Fig. 7 the values of h_1 are plotted as a function of H for different choices of the Bond number B_0.

The numerical procedure presented in this work allows one to calculate the temporal evolution of the interface shape and the velocity field for arbitrary impulsive conditions. For the sake of illustration, Fig. 8 shows the temporal evolution of the interface shape given by the first oscillation mode of a non-cylindrical liquid bridge for $\mathcal{B} = 1$ (impulsive motion).

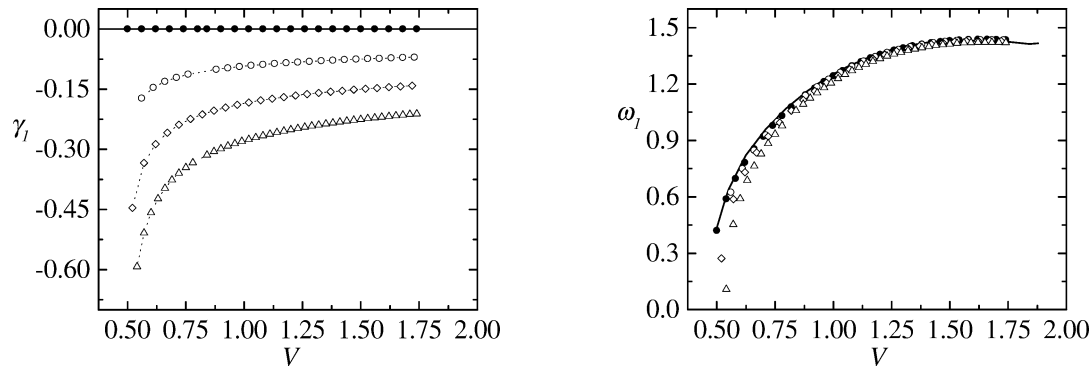

Fig. 6. Pole $h_1 = \gamma_1 + \mathrm{i}\omega_1$ as a function of the volume V for $\Lambda = 1.6$, $B_0 = H = W = 0$. The symbols are the results obtained from the Cosserat model for $C = 0$ (●), 0.05 (○), 0.1 (◇) and 0.15 (△), while the solid lines represent the results obtained by means of the 3-D model for $C = 0$.

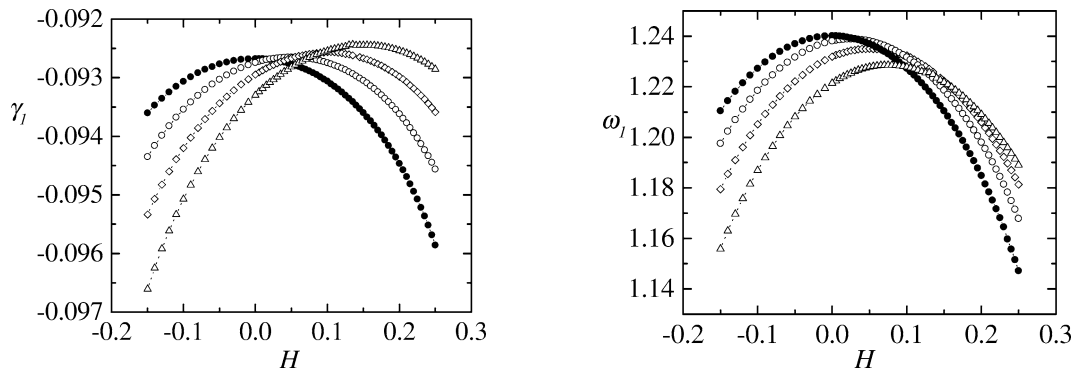

Fig. 7. Pole $h_1 = \gamma_1 + i\omega_1$ as a function of H for $\Lambda = 1.6$, $V - 1 = W = 0$, $C = 0.05$ and $B_0 = 0$ (●), 0.05 (○), 0.1 (◇) and 0.15 (△).

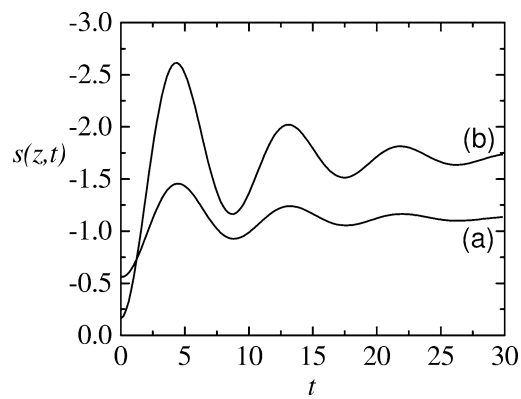

Fig. 8. Temporal evolution of the interface shape $s(z,t)$ for $\mathcal{B} = 1$, $\Lambda = 2$, $V - 1 = H = W = 0$, $B_0 = 0.05$, $C = 0.1$ and $z = \Lambda/4$ (a) and $z = \Lambda/2$ (b).

References

[1] T.Y. Chen, J. Tsamopolous, Nonlinear dynamics of capillary bridges: theory, J. Fluid Mech. 255 (1993) 373–409.
[2] A. Sanz, The influence of the outer bath in the dynamics of axisymmetric liquid bridges, J. Fluid Mech. 156 (1985) 101–140.
[3] J.A. Nicolás, Hydrodynamic stability of high-viscosity cylindrical liquid bridges, Phys. Fluids A 4 (1992) 1620–1626.
[4] M. Higuera, J.A. Nicolás, J.M. Vega, Linear oscillations of weakly dissipative axisymmetric liquid bridges, Phys. Fluids 6 (1994) 438–450.
[5] J.A. Nicolás, D. Rivas, J.M. Vega, On the steady streaming flow due to high-frequency vibration nearly inviscid liquid bridges, J. Fluid Mech. 354 (1998) 147–174.

[6] J.A. Nicolás, J.M. Vega, Linear oscillations of axisymmetric viscous liquid bridges, Z. Angew. Math. Phys. 51 (2000) 701–731.
[7] A.E. Green, On the nonlinear behaviour of fluid jets, Int. J. Eng. Sci. 14 (1976) 49–63.
[8] F.J. García, A. Castellanos, One-dimensional models for slender axisymmetric viscous liquid bridges, Phys. Fluids 8 (1996) 2837–2846.
[9] F.J. García, A. Castellanos, H. González, Dynamics of slender liquid bridges subjected to axial AC fields, J. Electrostatics 42 (1997) 259–278.
[10] J.M. Perales, J. Meseguer, Theoretical and experimental study of the vibration of axisymmetric viscous liquid bridges, Phys. Fluids A 4 (1992) 1110–1130.
[11] J.M. Montanero, Theoretical analysis of the vibration of axisymmetric liquid bridges of arbitrary shape, Theor. Comput. Fluid Dynamics 16 (2003) 171–186.
[12] F. Zayas, J.I.D. Alexander, J. Meseguer, J.F. Ramus, On the stability limits of long nonaxisymmetric cylindrical liquid bridges, Phys. Fluids 12 (2000) 979–985.
[13] J.M. Montanero, G. Cabezas, J. Acero, J.M. Perales, Theoretical and experimental analysis of the equilibrium contours of liquid bridges of arbitrary shape, Phys. Fluids 14 (2002) 682–693.
[14] J. Meseguer, J.M. Perales, N.A. Bezdenejnykh, A theoretical approach to impulsive motion of viscous liquid bridges, Microgravity Q. 1 (1991) 215–219.
[15] R.M.S.M. Schulkes, Nonlinear dynamics of liquid columns: a comparative study, Phys. Fluids A 5 (1993) 2121–2130.
[16] W.R. Lepage, Complex Variables and the Laplace Transform for Engineers, Dover, New York, 1980.
[17] J. Meseguer, J.M. Perales, A linear analysis of g-jitter effects on viscous cylindrical liquid bridges, Phys. Fluids A 3 (1991) 2332–2336.
[18] J. Meseguer, J.M. Perales, Nonsteady phenomena in the vibration of viscous, long liquid bridge, Microgravity Sci. Tech. 5 (1992) 69–72.
[19] R. Monti, R. Savino, G. Alterio, Modelling and simulation of g-jitter effects on fluid science experimentation. Impact on the utilization of the ISS, Acta Astronautica 40 (1997) 369–381.
[20] S. Wolfram, The Mathematica Book, Wolfram Media/Cambridge University Press, Cambridge, 1999.
[21] J. Abate, W. Whitt, The Fourier-series method for inverting transforms of probability distributions, Queueing Systems 10 (1992) 5–88.